Supporting Information

One-Step Synthesis of Porous Transparent Conductive Oxides by Hierarchical Self-Assembly of Aluminium-Doped ZnO Nanoparticles

Renheng Bo[1,#], Fan Zhang[1,2,3,#], Shulin Bu[1], Noushin Nasiri[1,4], Iolanda Di Bernardo[1], Thanh Tran-Phu[1], Aabhash Shrestha[1], Hongjun Chen[1], Mahdiar Taheri[5], Shuhua Qi[2], Yi Zhang[3], Hemant Kumar Mulmudi[1], Josh Lipton-Duffin[6], Enrico Della Gaspera[7], Antonio Tricoli[1, *]

[1]Nanotechnology Research Laboratory, Research School of Engineering, Australian National University, Canberra 2601, Australia

[2]Department of Applied Chemistry, Northwestern Polytechnical University, Xi'an, China

[3]College of Energy Engineering, Nanjing Tech University, Nanjing, China

[4]School of engineering, Macquarie University, Sydney, NSW 2109, Australia

[5]Labotatory of Advanced Nanomaterials for Sustainability, Research School of Engineering, Australian National University, Canberra 2601, Australia

[6]Institute for Future Environments (IFE) and Central Analytical Research Facility (CARF), Queensland University of Technology (QUT), Level 6, P Block, Gardens Point campus, 2 George St Brisbane QLD 4000

[7]School of Science, RMIT University, Melbourne, Victoria 3000, Australia

*Corresponding author: Antonio Tricoli
E-mail: antonio.tricoli@anu.edu.au
Tel: +61 2 6125 16

[#]Renheng Bo and Fan Zhang contributed equally in this work

Cross-sectional SEM image of an optimal AZO film (1 mol% AZO with 98% porosity) shows that there is no visible cracks found over hundreds of micro meters.
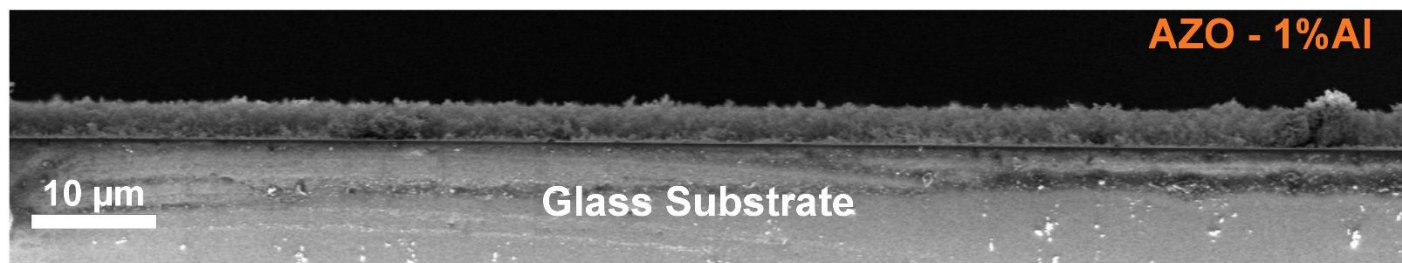

Figure S1 SEM cross-section image of the Al-ZnO film with no visible cracks and other defects on glass substrate.

In order for a clear comparison, all of the pure ZnO and AZO films (1 to 10 mol% Al concentrations) are kept identical in terms of structural properties (approx. 7 μm thick with 98 % porosity) for XPS survey spectra measurements.
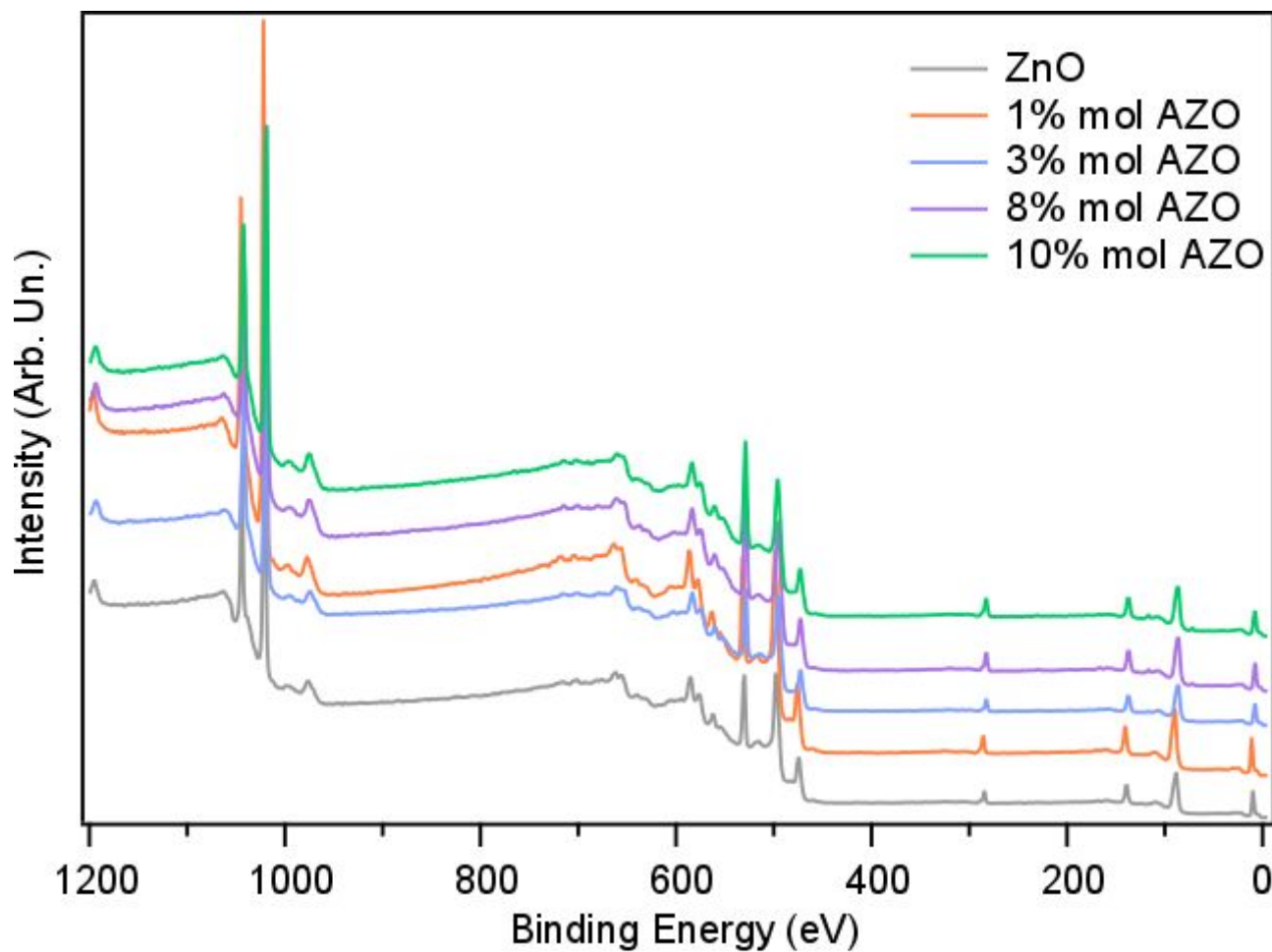

Figure S2 XPS survey spectra for pure ZnO and 1 to 10 mol% AZO.

The FTIR spectra were further analysed to verify the successful incorporation of Al in the ZnO nanoparticles. All the Al-doped particles exhibit a characteristic peak at 683 cm^{-1} (Fig. S3), which is regarded as a finger print of Al-O bond[1] and indicates the presence of Al in the samples. The peaks at 550-437 cm^{-1} correspond to the formation of Zn-O bonds.[2] In addition, a broad absorption peak at 3445 cm^{-1} and the corresponding peaks at 1637 cm^{-1} and 1110 cm^{-1} can be assigned to the O-H bonds.[3] The small peaks at 1540 cm^{-1}, 1480 cm^{-1} and 800 cm^{-1} are due to the absorption of atmospheric CO_2 on the metal cations.[4]
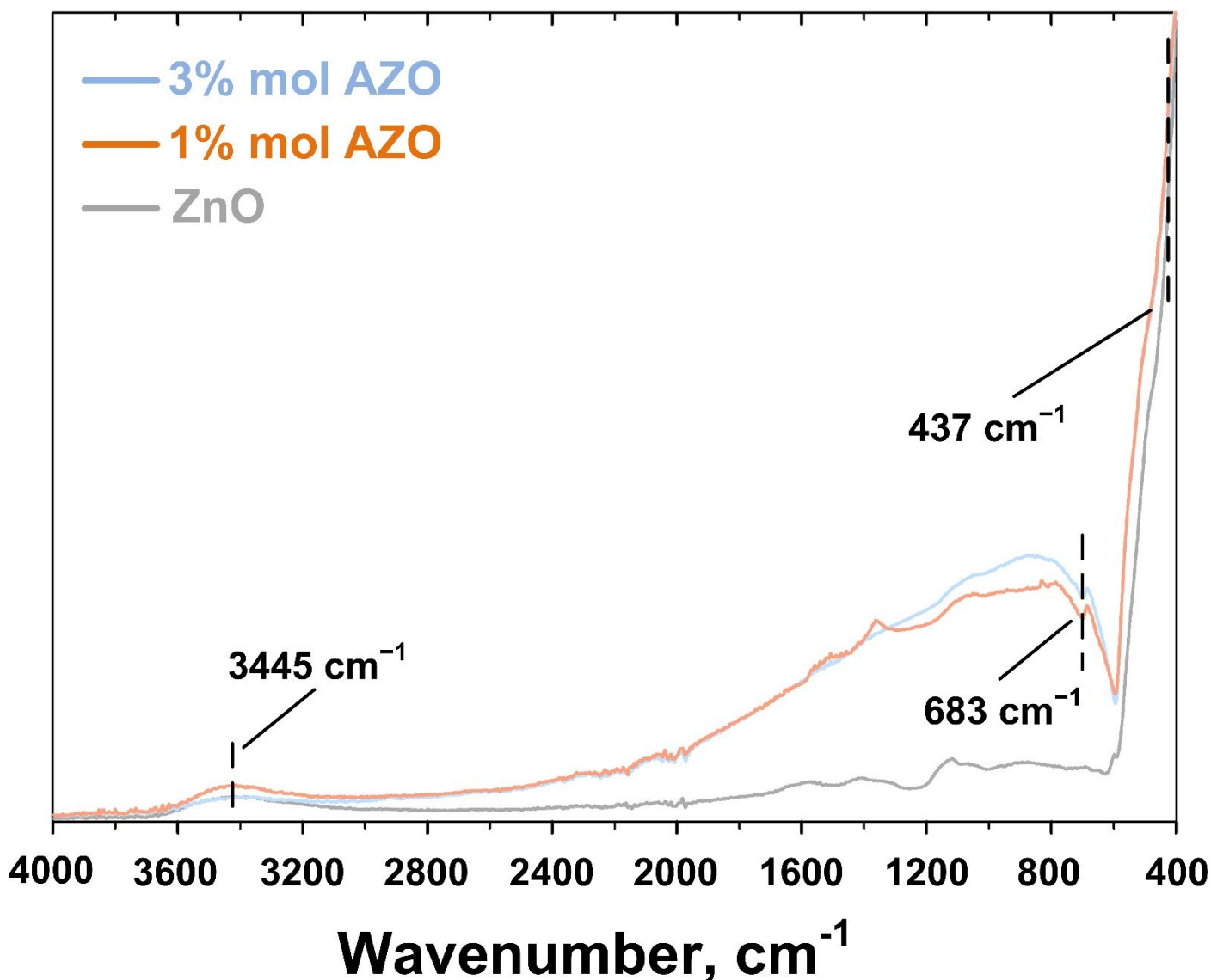
Figure S3 FTIR of pure ZnO, 1 mol% AZO and 3 mol% AZO. In order for a clear comparison, all of the pure ZnO and AZO films (1 to 10 mol% Al concentrations) are kept identical in terms of structural properties (approx. 7 μm thick with 98 % porosity) for FTIR measurements.
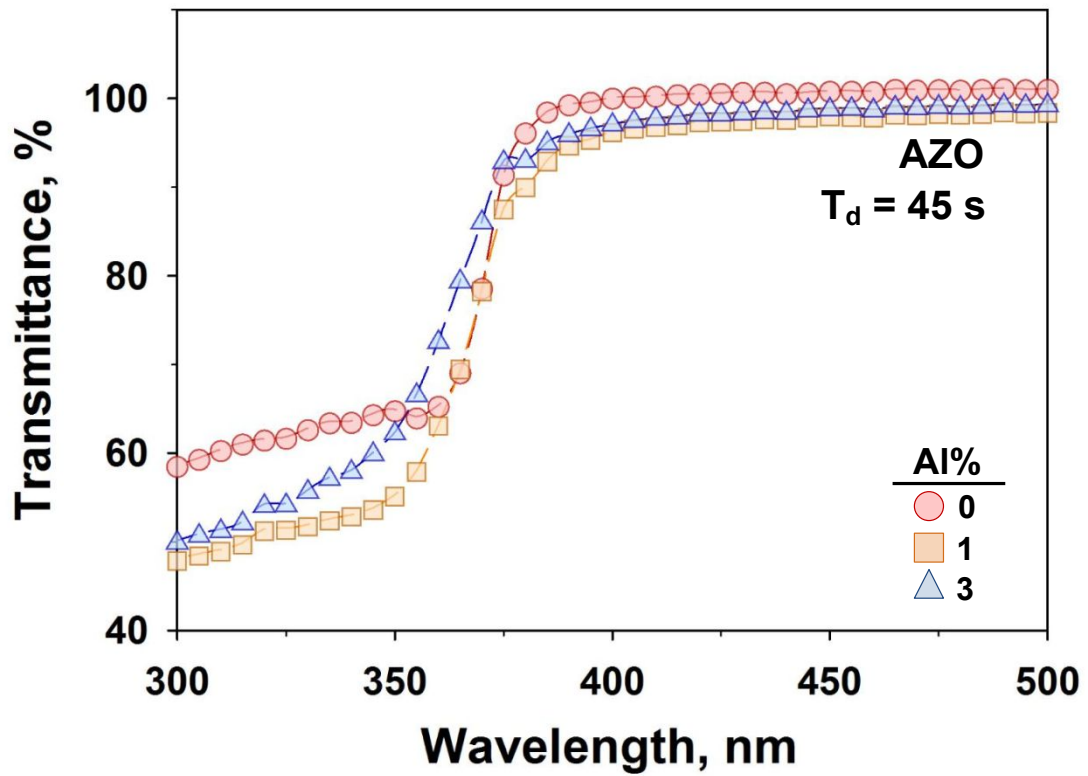
Figure S4 Optical transmittance spectra of the ultra-porous ZnO and AZO TEs (1 to 3 mol%). All films have identical structural property of 98 % porosity, 4.5 μm in thickness.

The optical transmittance spectra of the devices after subtraction of the fraction loss through the glass substrate are presented. The film average integral transmittance for both UV and visible light is computed by subtraction of the fraction lost through the glass substrates as follows:[5]

$$T_{Film} = I_{Film}/T_{Glass} \times 100 \tag{1}$$

where T_{Film} is the film average transmittance, I_{Film} is the transmittance through the glass and the film, and T_{Glass} is the glass transmittance.

Comparing to other AZO TEs (10 to 90 % porosities), the 98 % ones gives the lowest transparency (Fig. S9), therefore, only the transmittance of ultra-porous AZO (98 % porosity) has been measured to confirm the efficient transparency of our AZO TEs within visible spectra range (400 to 700 nm).

All of the emploed films have the same structural properties of 98 % porosity and approx 4.5 μm in thickness (Fig. S5).
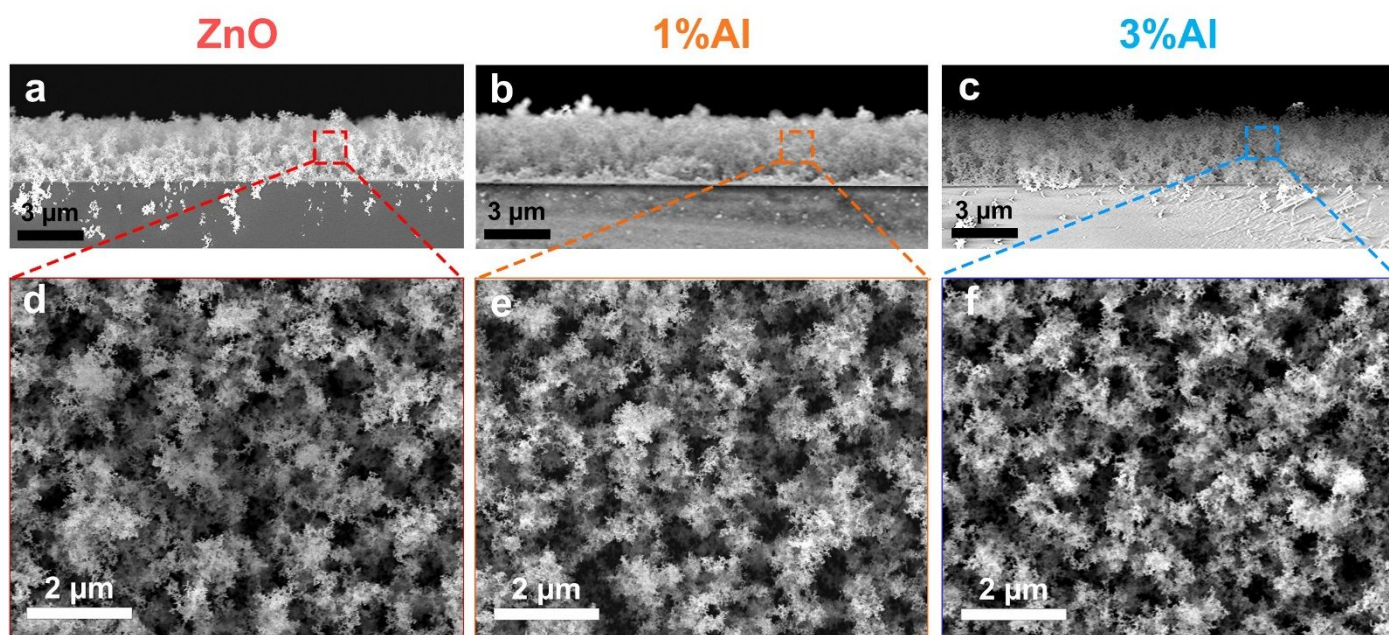
Figure S5 SEM images of pure ZnO, 1 mol% AZO and 3 mol% AZO ultra-porous films. SEM cross-section images of a) ZnO, b) ZnO with 1 mol% Al and c) ZnO with 3 mol% Al together with top-view images of d) ZnO, e) ZnO with 1 mol% Al and f) ZnO with 3 mol% Al.

The employed 1 mol% AZO ultra-porous film has a good photo-response as following which ensures the light-driven sensing mechanisms.
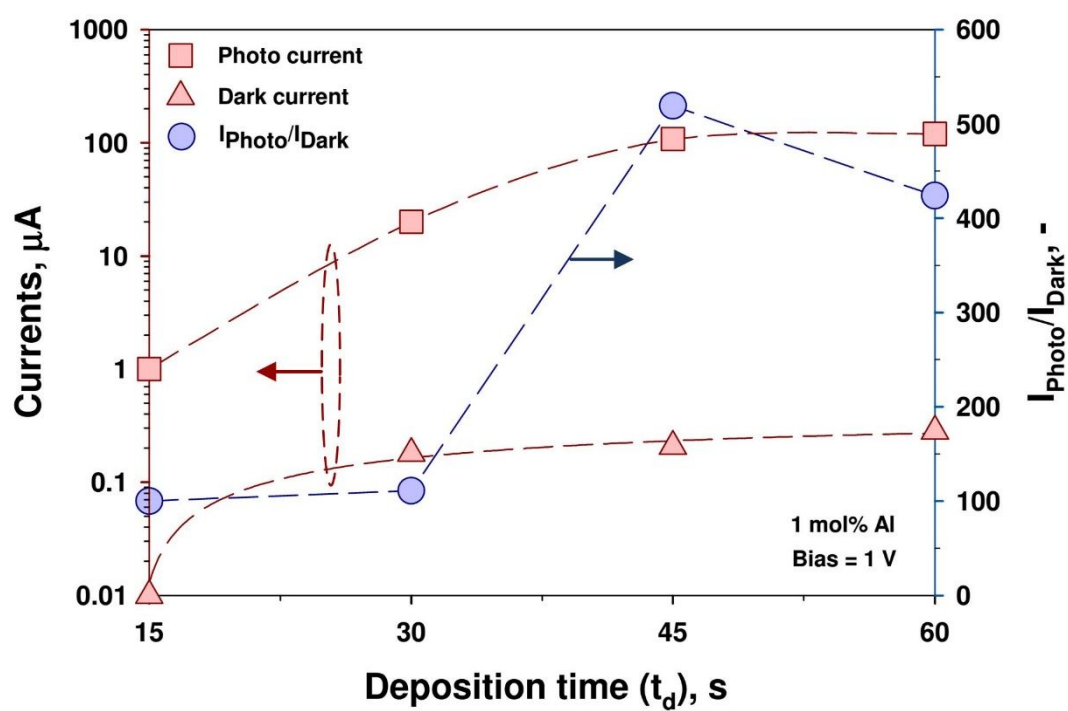

Figure S6 Photo-response of 1 mol% AZO ultra-porous film.

The sensing dynamics of 1 mol% AZO with/without illumination are in agreement with its photo-response (Fig. S6) which indicates a good light-driven behaviour.
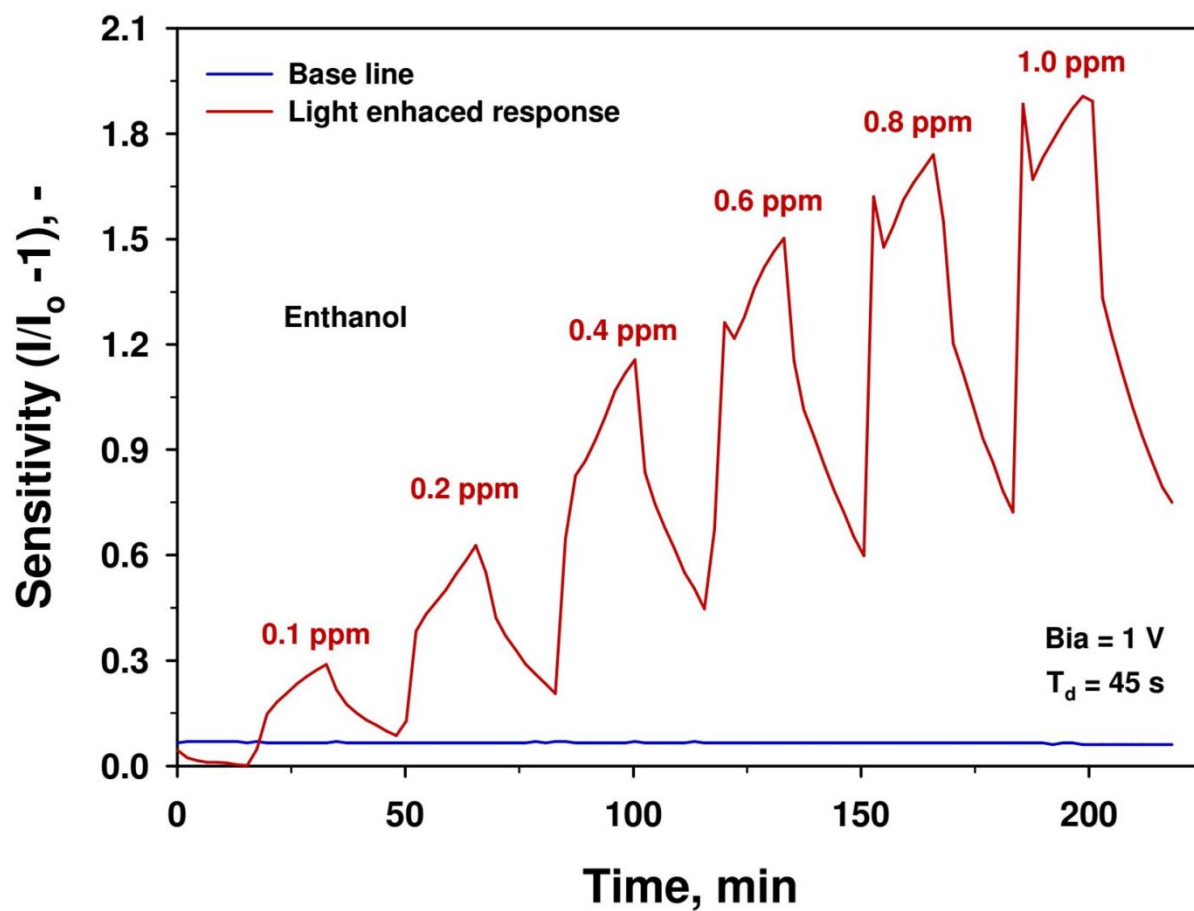
Figure S7 Sensing dynamics of 1 mol% AZO to ethanol with/without light.

In order to find the optimal thickness of 1 mol% AZO sensor, varied thicknesses from 1.5 to 6.0 μm have been prepared by the one-step FSP approach resulting in different sensitivities towards ethanol gas while increasing the gas concentration from 0.1 to 1.0 ppm. These results indicate an optimal thickness of 4.5 μm for 1 mol% AZO ultra-porous gas sensors.
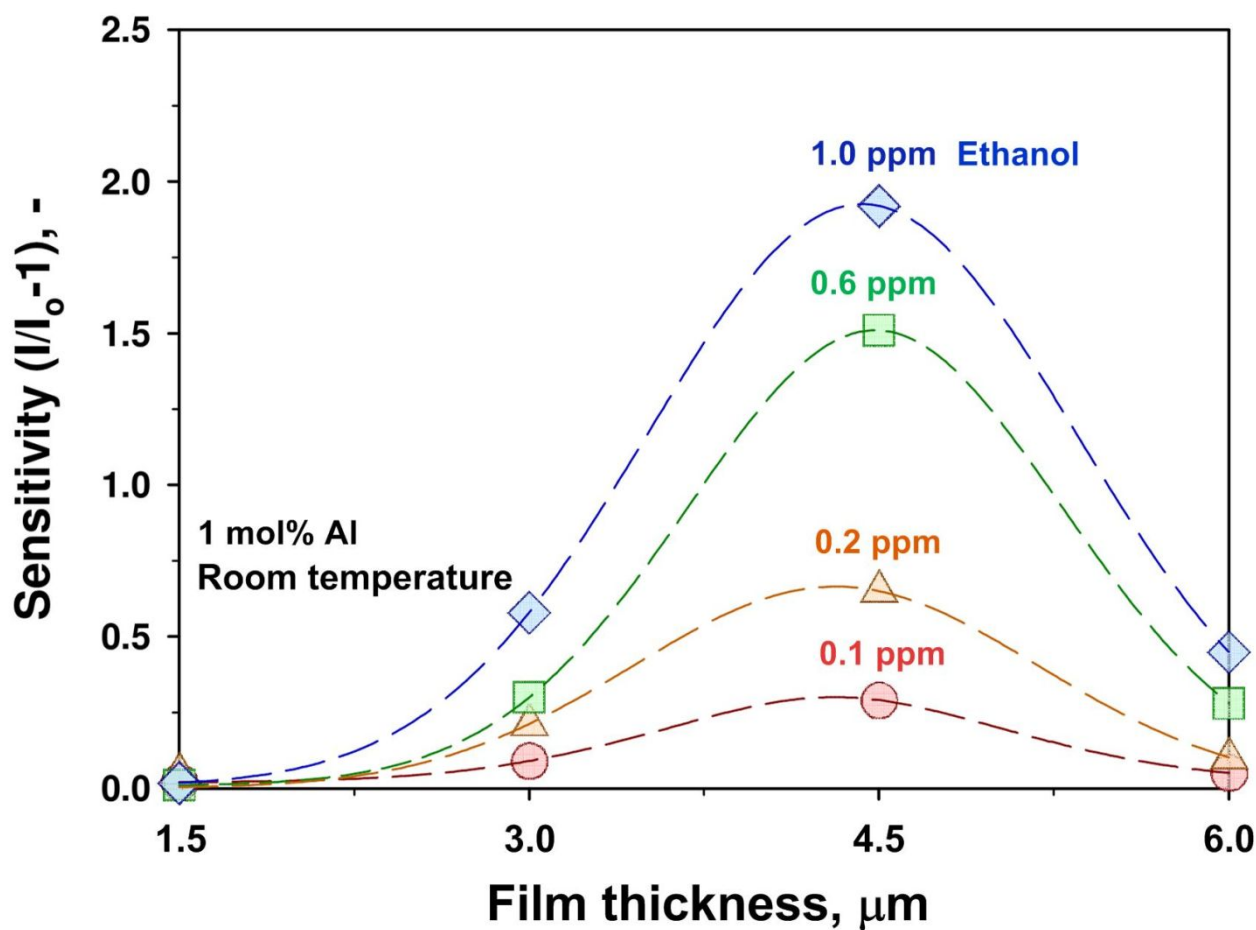
Figure S8 Sensing dynamics of 1 mol% AZO to ethanol with varied thickness.

All of the TEs (Fig. S9) are FPS 1 mol% AZO with varied porosities from 98 to 10 % from left to right. The reduced whiteness from left to right shows an increased transparency. Therefore, only AZO films with 98 % were measured for transmittance indicating a >85 % transmittance (Fig. S4) within the visible spectra range (400 to 700 nm).
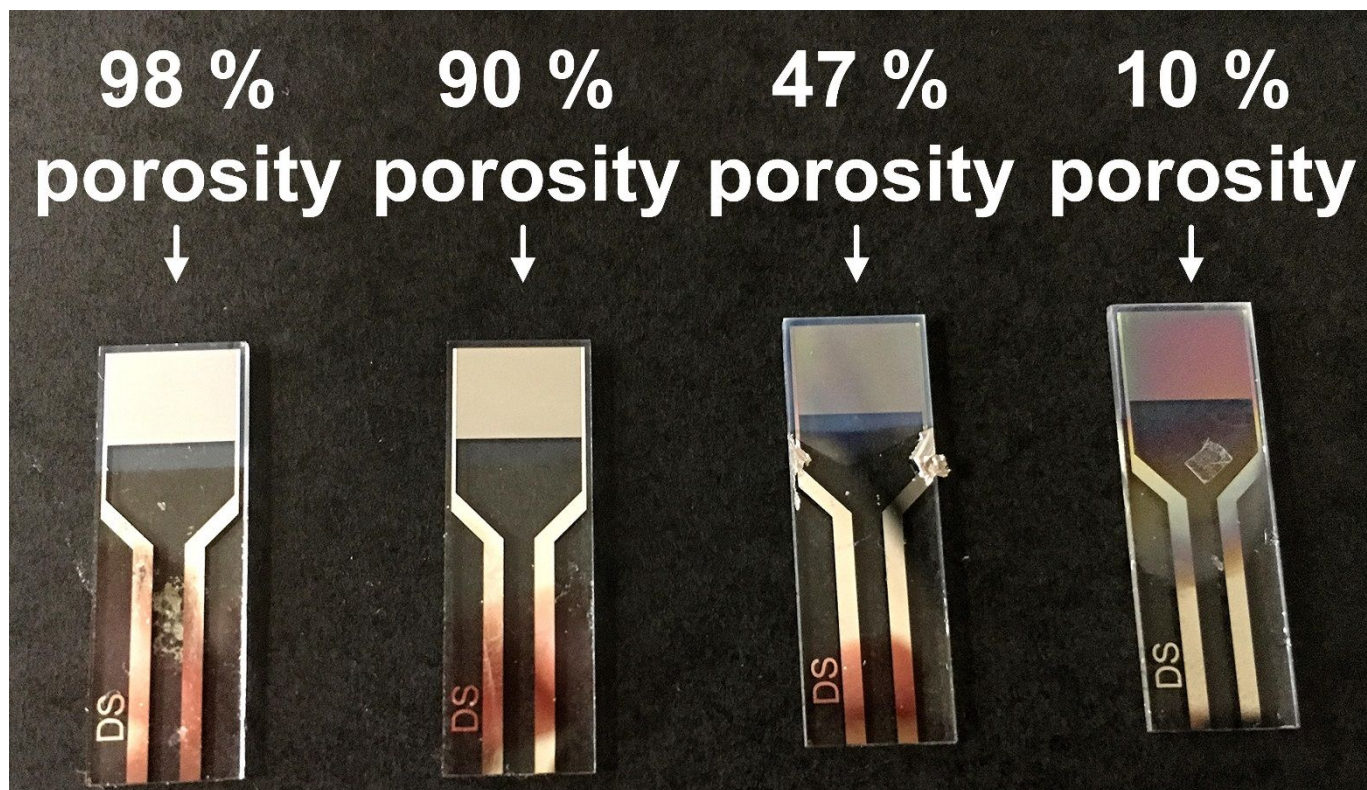
Figure S9 Photographs of AZO TEs with varied porosities (10 to 98 %). All of the films are the same ones in Fig. 3c-f.
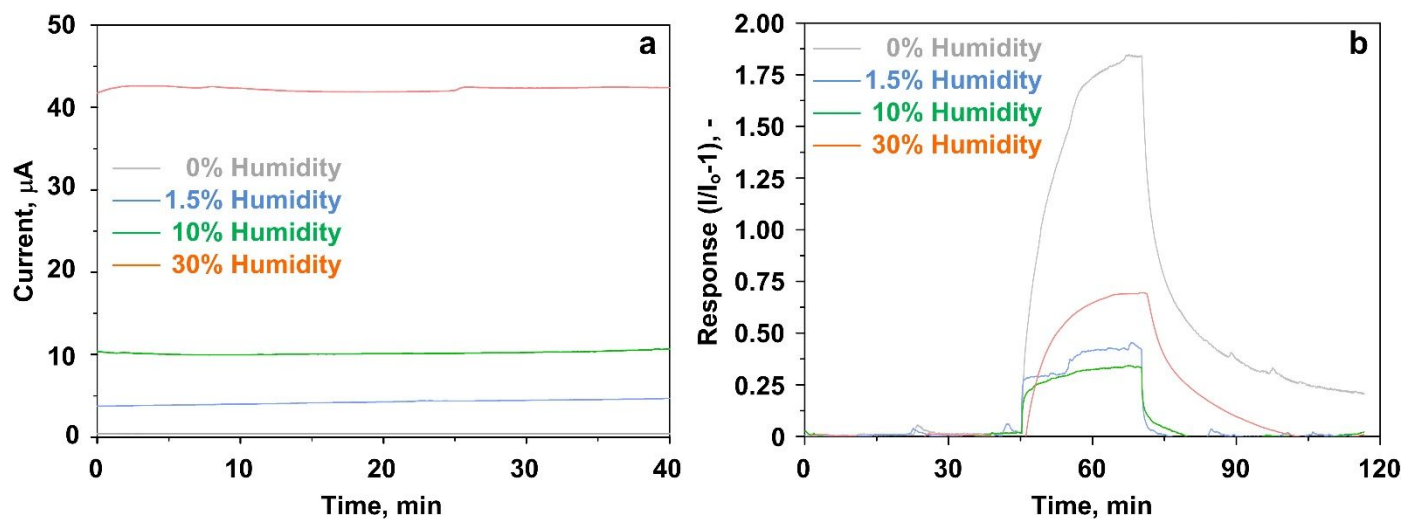
Figure S10. Effect of humidity on sensing performance. a) Base line of the optimal sensor (1 mol% AZO with 98% porosity) as a function of humidity. b) Dynamic response towards 1 ppm ethanol of the optimal sensor (1 mol% AZO with 98% porosity) as a function of humidity.
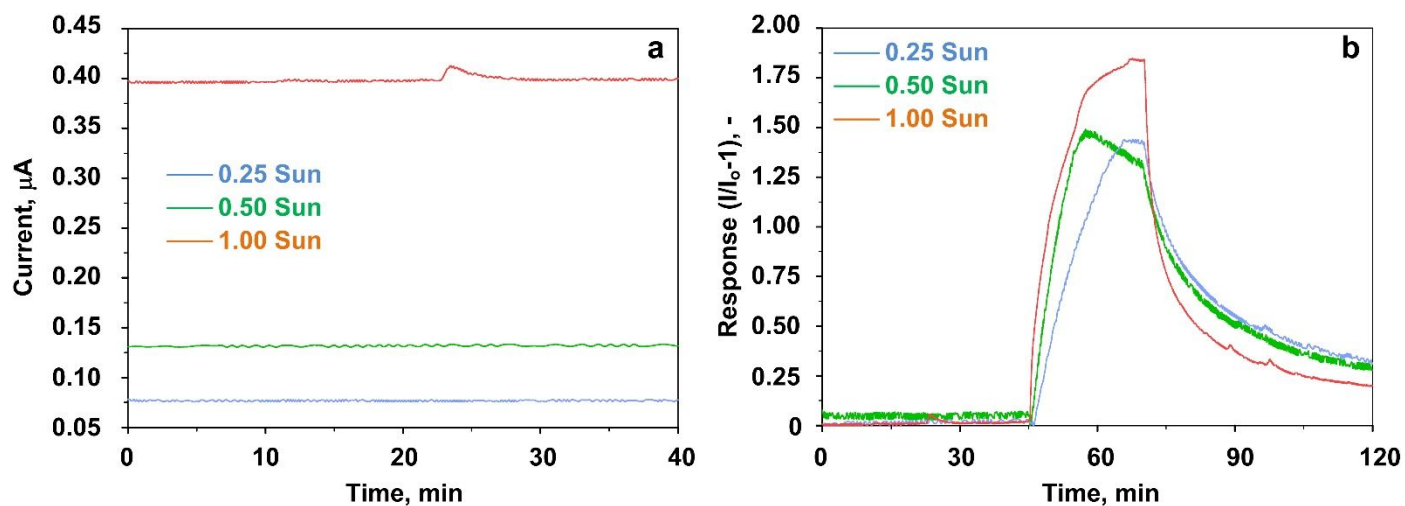
Figure S11. Effect of light intensity on sensing performance. a) Base line of the optimal AZO sensor (1 mol% AZO with 98% porosity) as a function of light intensity. b) Dynamic response towards 1 ppm ethanol of the optimal sensor (1 mol% AZO with 98% porosity) as a function of light intensity.

Table S1. XRD shifts of AZO films.

Material	Crystal Plane		
	(100)	**(002)**	**(101)**
ZnO	32°	34.6°	36.44°
1 mol% AZO	32.04°	34.62°	36.48°
3 mol% AZO	32.10°	34.66°	36.50°
8 mol% AZO	32.10°	34.66°	36.50°
10 mol% AZO	32.10°	34.66°	36.50°

Table S2 State-of-art light-driven gas sensors.

Material	Synthetic method	Sensitivity (-) to [concentration] analyte	illumination	Ref.
AZO with 1 mol.% Al film	Flame spray pyrolysis	(0.29) to [0.1 ppm] ethanol (1.92) to [1.0 ppm] ethanol	sunlight@1 sun AM 1.5	this work
AZO film with 2.9 at. Al	Chemical bath deposition	(0.953) to [25000 ppm] ethanol	/	[6]
ZnO–CuO	hydrothermal method	(1.3) to [150 ppm] ethanol	/	[7]
ZnO nanowire	/	(0.125) to [100 ppm] ethanol	UV@67.5 mW·cm^{-2} ;	[8]
SnO$_2$ Doped Poly-Diallyldimethylammonium Chloride	/	(~0.17) to [10 ppm] ethanol	/	[9]
Si nanoporous pillar array	hydrothermally etching	(~0.07) to [50 ppm] ethanol	/	[10]
Co$_3$O$_4$/Ta$_2$O$_5$ heterostructure hollow nanospheres	Solution mixing and annealing	(0.20) to [10 ppm] ethanol	/	[11]
ZnO/MWNTs film	layer-by-layer self-assembly technique	(0.016) to [5 ppm] ethanol	/	[12]
Ag@SnO$_2$ core–shell material	chemical reduction	(1.24) to [200 ppm] ethanol	/	[13]
TiO$_2$	/	(224.0) to [100 ppm] ethanol	UV	[14]
ZnO	/	(0.1) to [30 ppm] ethanol	UV	[14]
SnO$_2$ nanoribbon	Thermal deposition	(0.16) to [3 ppm] NO$_2$	365 nm@0.5 mW·cm^{-2}	[15]
SnO$_2$	DC magnetron sputtering	(16.0) to [1 ppm] NO$_2$ (0.63) to [100 ppm] CO	365 nm@0.5 mW·cm^{-2}	[16]
In$_2$O$_3$	RF magnetron sputtering	(28.0) to [3 ppm] NO$_2$ (0.23) to [50 ppm] CO	365 nm@0.5 mW·cm^{-2}	[16]
palladium loaded single-walled carbon nanotube	sputtering	(~0.02) to [6 ppm] methanol	254 nm	[17]
floccule-like zinc oxide nanostructures	self-aggregation	(0.2) to [2000 ppm] octane	UV	[18]

Table S3 XPS survey spectra.

Material	Element			
	O 1s	C 2p	Zn 2p	Al 2p
ZnO	39.43	19.34	38.04	0
1 mol% AZO	39.91	19.2	37.78	0
3 mol% AZO	41.56	20.56	34.83	0
8 mol% AZO	43.14	22.51	29.23	2.71
10 mol% AZO	43.55	22.35	28.77	3.06

Reference

1. Yogamalar, N. R.; Bose, A. C., Absorption-Emission Study of Hydrothermally Grown Al: ZnO Nanostructures. *J. Alloys Compd.* **2011,** *509* (34), 8493-8500.

2. Alias, S.; Ismail, A.; Mohamad, A., Effect of pH on ZnO Nanoparticle Properties Synthesized by Sol-Gel Centrifugation. *J. Alloys Compd.* **2010,** *499* (2), 231-237.

3. Mallika, A.; RamachandraReddy, A.; SowriBabu, K.; Reddy, K. V., Synthesis and Optical Characterization of Aluminum Doped ZnO Nanoparticles. *Ceram. Int.* **2014,** *40* (8), 12171-12177.

4. Pholnak, C.; Sirisathitkul, C.; Suwanboon, S.; Harding, D. J., Effects of Precursor Concentration and Reaction Time on Sonochemically Synthesized ZnO Nanoparticles. *Mater. Res.* **2014,** *17* (2), 405-411.

5. Bo, R.; Nasiri, N.; Chen, H.; Caputo, D.; Fu, L.; Tricoli, A., Low-Voltage High-Performance UV Photodetectors: An Interplay Between Grain Boundaries and Debye Length. *ACS Appl. Mater. Interfaces* **2017,** *9* (3), 2606-2615.

6. Nulhakim, L.; Nugraha; Nuruddin, A.; Suyatman; Yuliarto, B. In *Al-Doped ZnO Thin Films for Ethanol Sensors*, AIP Conference Proceedings, AIP: **2011**; pp 227-230.

7. Yu, M.-R.; Suyambrakasam, G.; Wu, R.-J.; Chavali, M., Performance Evaluation of ZnO-CuO Hetero Junction Solid State Room Temperature Ethanol Sensor. *Mater. Res. Bull.* **2012,** *47* (7), 1713-1718.

8. Wang, P.; Fu, Y.; Yu, B.; Zhao, Y.; Xing, L.; Xue, X., Realizing Room-Temperature Self-powered Ethanol Sensing of ZnO Nanowire Arrays by Combining Their Piezoelectric, Photoelectric and Gas Sensing Characteristics. *J. Mater. Chem. A* **2015,** *3* (7), 3529-3535.

9. Zhan, S.; Li, D.; Liang, S.; Chen, X.; Li, X., A Novel Flexible Room Temperature Ethanol Gas Sensor Based on SnO_2 Doped Poly-diallyldimethylammonium Chloride. *Sensors* **2013,** *13* (4), 4378-4389.

10. Li, X. J.; Chen, S. J.; Feng, C. Y., Characterization of Silicon Nanoporous Pillar Array as Room-Temperature Capacitive Ethanol Gas Sensor. *Sens. Actuators, B* **2007,** *123* (1), 461-465.

11. Zhang, Z.; Wen, Z.; Ye, Z.; Zhu, L., Synthesis of Co_3O_4/Ta_2O_5 Heterostructure Hollow Nanospheres for Enhanced Room Temperature Ethanol Gas Sensor. *J. Alloys Compd.* **2017**.

12. Zhang, D.; Sun, Y. E.; Zhang, Y., Fabrication and Characterization of Layer-by-layer Nano Self-Assembled ZnO Nanorods/Carbon Nanotube Film Sensor for Ethanol Gas Sensing Application at Room Temperature. *J. Mater. Sci-Mater. El.* **2015,** *26* (10), 7445-7451.

13. Liu, J.; Lu, R.; Xu, G.; Wu, J.; Thapa, P.; Moore, D., Development of a Seedless Floating Growth Process in Solution for Synthesis of Crystalline ZnO Micro/Nanowire Arrays on Graphene: Towards High-Performance Nanohybrid Ultraviolet Photodetectors. *Adv. Funct. Mater.* **2013,** *23* (39), 4941-4948.

14. Chen, H.; Liu, Y.; Xie, C.; Wu, J.; Zeng, D.; Liao, Y., A Comparative Study on UV Light Activated Porous TiO_2 and ZnO Film Sensors for Gas Sensing at Room Temperature. *Ceram. Int.* **2012,** *38* (1), 503-509.

15. Law, M.; Kind, H.; Messer, B.; Kim, F.; Yang, P., Photochemical Sensing of NO_2 with SnO_2 Nanoribbon Nanosensors at Room Temperature. *Angew. Chem.* **2002,** *41* (13), 2405-8.

16. Comini, E.; Cristalli, A.; Faglia, G.; Sberveglieri, G., Light Enhanced Gas Sensing Properties of Indium Oxide and Tin Dioxide Sensors. *Sens. Actuators, B* **2000,** *65* (1–3), 260-263.

17. Lu, Y.; Li, J.; Han, J.; Ng, H. T.; Binder, C.; Partridge, C.; Meyyappan, M., Room Temperature Methane Detection Using Palladium Loaded Single-walled Carbon Nanotube Sensors. *Chem. Phys. Lett.* **2004,** *391* (4), 344-348.

18. Ho, Y. H.; Huang, W. S.; Chang, H. C.; Wei, P. K.; Sheen, H. J.; Tian, W. C., Ultraviolet-Enhanced Room-Temperature Gas Sensing by Using Floccule-like Zinc Oxide Nanostructures. *Appl. Phys. Lett.* **2015,** *106* (18), 15.